The influence of grain boundaries and grain orientations on the stochastic responses to low load nanoindentation in Cu

B.J. Schuessler, P.C. Wo, H.M. Zbib

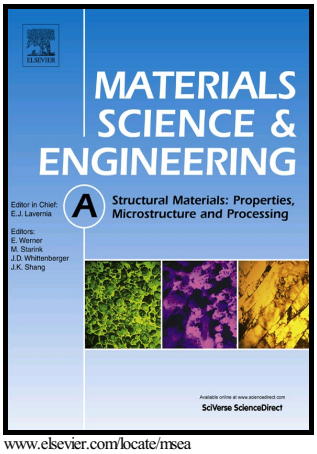

www.elsevier.com/locate/msea

PII: S0921-5093(18)30010-8
DOI: https://doi.org/10.1016/j.msea.2018.01.009
Reference: MSA35963

To appear in: *Materials Science & Engineering A*

Received date: 8 June 2017
Revised date: 3 January 2018
Accepted date: 3 January 2018

Cite this article as: B.J. Schuessler, P.C. Wo and H.M. Zbib, The influence of grain boundaries and grain orientations on the stochastic responses to low load nanoindentation in Cu, *Materials Science & Engineering A,* https://doi.org/10.1016/j.msea.2018.01.009

The influence of grain boundaries and grain orientations on the stochastic responses to low load nanoindentation in Cu

B. J. Schuessler, P.C. Wo*, H.M. Zbib

School of Mechanical and Materials Engineering

Washington State University, Pullman, WA

Abstract

Mechanical properties that are considered to be deterministic in the macro-scale have been shown to be stochastic in the sub-micron length scale. The origin of such stochastic responses is not well understood. This work examines the potential influence of grain boundaries and grain orientations on the stochastic nature of pop-in and hardness measurement in annealed high purity polycrystalline Cu samples during low load nanoindentation. Statistical analysis on pop-in load and hardness showed that variations of these measurements depend on crystal orientations and is influenced by the indenter probe size. Analysis on the pop-in load statistics showed that pop-ins are likely initiate from an atomic sized precursor that leads to dislocation generation or expansion. Variation in hardness measurements near an arbitrary chosen grain boundary and the apparent grain boundary hardening effect observed may be related to the higher density of dislocations at and near the grain boundary.

Keywords: *nanoindentation, stochasticity, hardness, pop-in, microstructure*

*Corresponding Author

Introduction

Traditionally thought, mechanical properties are constant throughout all length scales. Yet, it has been observed that mechanical properties of materials in sub-micron scales begin to deviate from their macro-scale behaviors. Properties such as, hardness, *H*, and elastic modulus, *E*, are observed to display a noticeable scattering while undergoing nanoindentation testing [1-4]. The onset of plasticity, seen in the form of "pop-in" under load-controlled nanoindentation in relatively defect-free metallic crystals [5-7], has also been observed to be stochastic [3, 8-11] and even time dependent [10, 12]. Although data scattering phenomenon in low-load nanoindentation has been often attributed to extrinsic factors and was commonly considered to be scattering noise, recent molecular dynamics (MD) simulations suggested that such stochastic behavior can be associated with the intrinsic property of the testing material, for example, the type, ordination and position of defects that may exist under the indenter [13]. In particular, discrete dislocation dynamics developed to study micropillar compression suggested that spatial distribution and density of initial dislocation both contribute to the stochastic nature of the onset of plasticity [14]. On the other hand, data variation and the mean values of pop-in loads are shown to be both depending on other intrinsic properties, such as crystal orientation [8, 13, 14] and testing conditions such as tip size [8]. In addition, tips having larger radii are found to be more sensitive to crystal orientation and may yield at a lower applied stress [8].

This study investigates how microstructure, in particularly crystal orientation and grain boundaries, affects the stochasticity of the onset of plastic deformation and *H* in the sub-micron scale. Nanoindentation tests were performed on three large grains arbitrarily chosen without specific orientation preferences from a well-annealed polycrystalline copper sample to study the effect of crystal orientation on pop-in load and pop-in excursions. Indentations were made using Berkovich tips having two different radii on these grains in order to study the influence of indenter radii on hardness and contribution to the stochasticity of its measurements. In addition, indentations were also carried out near and at varying distances away from a selected grain boundary to study their influence on the hardness measurements.

Experimental

Nanoindentation tests were performed on a 99.999% polycrystalline Cu foil prepared as follows. First the as-given Cu plate approximately 10 mm in diameter and 3 mm thick was annealed at 700°C for 72 hours then allowed to furnace cool. After cooling, the samples were mechanically ground to approximately 100 μm thick and then both sides of the foil were polished with 1200 grit sandpaper. Disks of 3 mm in diameter were punched out of the foil. These disks were then electropolished using an automatic twin-jet electropolisher for transmission electron microscopy (TEM) sample preparation (Model 110, Fischione instruments) using a 1:1 phosphoric acid and deionized water electrolyte at 3.5V for about 20 seconds at room temperature. To prepare samples suitable for nanoindentation, the surface on which nanoindentation to be performed were electropolished, but the opposite surface of the disk must remain flat. This can be done by isolating one side of the disk from the electrolyte using a thin layer of lacquer during electropolishing in the twin-jet setup. Samples having both sides electropolished were also prepared in order to examine the microstructure of the samples before nanoindentation tests in the TEM. A visually luminous surface can be seen after electropolish indicating a smooth surface. Microstructure of the initial, undeformed copper samples was examined using a Philips CM-200 TEM equipped with a double tilt holder.

The microstructure and indentations were observed in an FEI Sirion200 scanning electron microscope (SEM). This SEM is equipped with an electron backscatter diffraction (EBSD) detector, which facilitate crystal structure and orientation analysis. EBSD was performed using a step size of 2.25 μm to gather grain orientation data, from which grains suitable to perform indentation tests in the current studies were selected. Three grains, having different orientations, were qualitatively chosen based on the grain size for the nanoindentation test.

Nanoindentations were carried out on a Hysitron TI-900 TriboIndenter platform, which is capable of performing scanning probe microscopy (SPM) imaging with the indenter probe. By performing an SPM scan prior to indentation, the location of the indent could be made within 1-2 μm from the desired location. This capability of our nanoindentation system is particularly important in studying the grain boundary effects on the measured properties as indents could be placed from various distances near an identified grain boundary. Two Berkovich indentation probes having significantly different tip radii due to different wear conditions were used. Assuming that the deformation before the occurrence of pop-in is purely elastic and is fully

reversible, the initial loading segment of the load-displacement curve before the occurrence of a pop-in can be described by the Hertzian contact theory[15]:

$$P = \frac{4}{3} E^* \sqrt{Rh^3} \quad (1)$$

where P is the applied load, E^* is the reduced modulus, R is the indenter radius (the radius of a sphere that fits the roundness of the tip) and h is the indentation contact depth. Therefore, the indenter radius can be estimated by fitting the initial loading segment of the load-displacement curve obtained from an indentation test using a suitable value for R in equation (1). The value of R that yields the best fit of the curve segment is considered to be the indenter radius. Using the method described above, the radius of each of the two tips was estimated to be an average value obtained from five indentation curves. It is found that one of the indenter probes has a radius of 2420 ± 220 nm and the other has a radius of 353 ± 23 nm.

All indentations were made using a simple load-hold-unload profile. Load was applied at a constant rate of 417 μN/s to reach a maximum load, P_{max}, at 500 μN. The load was held at P_{max} for 10 seconds before unloading at a rate of -417 μN/s. There is at least 5 μm spacing between each indent in order to avoid influence from the previously made indent.

Grain Selection and Initial Microstructure Characterization

Two inverse pole figure representations of an EBSD scan of the electropolished sample surface are shown in Figure 1. It can be seen that typical grains are roughly equiaxial in shape. The average grain size is ~ 65 μm and some grains are > 100 μm. The grain orientations are found to be roughly random. Three grains, namely A, B and C (indicated in Figure 1), are selected for nanoindentations. Each of these grains has an area roughly equal to a circle 100 μm in diameter and was chosen mainly due to their large size rather than a specific grain orientation. Large grains are important for further nanoindentation testing as they offer larger area for indents to be placed within the grain and away from any grain boundary to avoid potential influence from them.

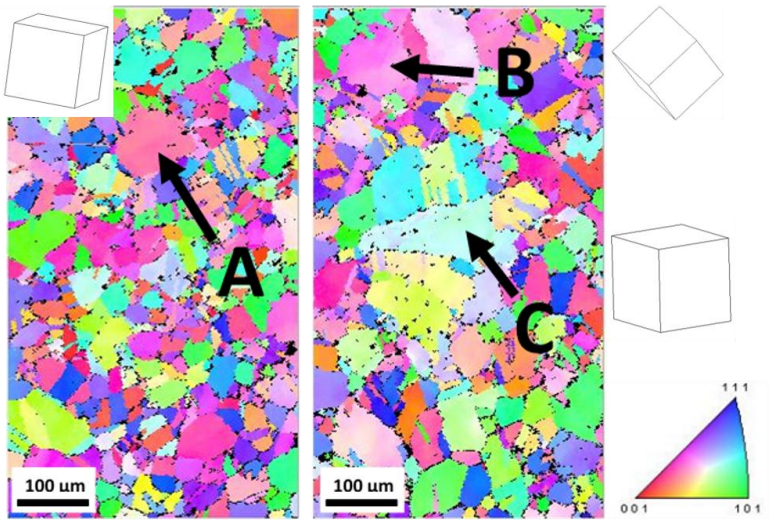

Figure 1. Inverse pole figure image of typical scanned areas in the as-prepared Cu sample showing grains A-C (arrowed) selected for nanoindentation tests. The lattice orientation for Grain A, B and C are also presented.

As-prepared samples that were electropolished on both sides of the 3mm disc were examined in the TEM to study the microstructure of the sample before nanoindentation tests. Typical bright field micrographs obtained from a sample are shown in Figure 2. Several isolated dislocations can be seen within a grain in Figure 2(a) and an array of dislocations that forms a band, which appears to have a finite thickness of ~ 125 nm can be seen (Figure 2(b)). Selected area diffraction patterns on the left and right of this array of dislocations are different, demonstrating that these dislocations are aligned along a grain boundary. Pre-existing dislocation density within the grains was determined to be approximately 2×10^{13} m^{-2}. This is an average value of dislocation density calculated from ten bright-field TEM micrographs taken at a magnification of 24,500x under a two-beam condition at different positions within various grains (without considering dislocation structures near or at grain boundaries as shown in Figure 2(b)). The dislocation density from each image was determined by counting the number of dislocation lines observed divided by the area of the region examined (~ 1.03 μm^2). Using this method, a dislocation is assumed to be a continuous line within the frame of the micrograph. Dislocations exhibiting curved or jagged lines and those that resembling a "dashed-line" were considered to be a single dislocation. The estimated dislocation density in the sample is two orders of magnitude higher than that suggested in the literature for well-annealed metallic single crystals (10^{11} m^{-2}) [16]. This higher dislocation density is likely the result of minor strain and deformation imposed on the material during sample processing, especially when the TEM discs

were punched out. As the current study aimed to investigate the influence of microstructure, including defects, on nanoindentation measurements, the higher initial dislocation density should not affect the quality of the investigation.

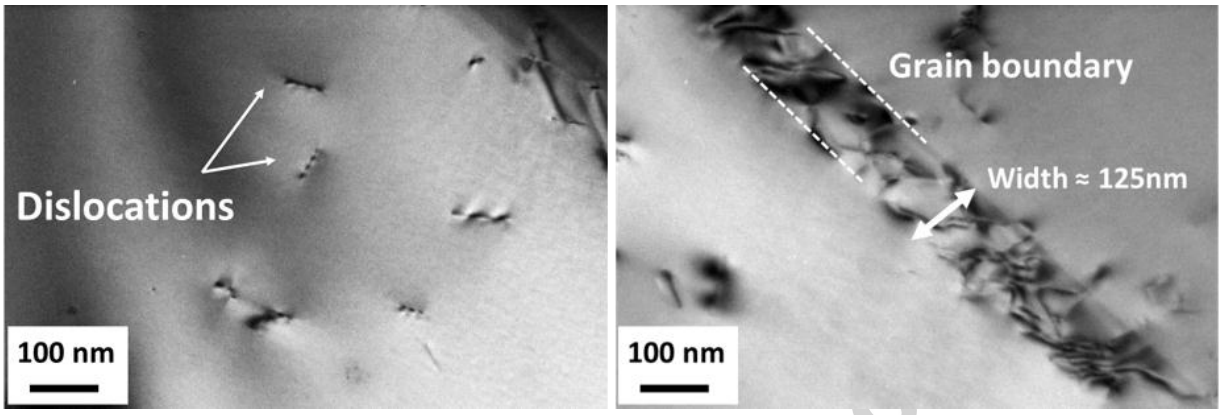

Figure 2. Transmission electron micrograph of a polycrystalline copper sample showing (a) isolated individual dislocations within the interior of a grain; (b) an array of dislocations forming a band that is ~ 125 nm wide along a grain boundary.

Effect of Grain Orientation on Pop-in Phenomena

In order to study the effect of grain orientations on the onset of plastic deformation during nanoindentation, 50 indents were performed using the smaller nanoindenter probe (R~353 nm) on each of the selected three grains indicated in Figure 1. All of the indents are at least 10 μm from a grain boundary in order to avoid potential influences from them. It should also be noted that the separation between each indentation is 5 μm, which is about five times the radius of a circle that have the same projected area of the indent and so influence from the plastic deformation of prior indents should be negligible. As discussed above, these grains were randomly selected based on their large size rather than a specific orientation. The normal of Grain A, B and C are found to be [5 -2 22], [-10 -28 -7] and [1 7 1], respectively. The lattice orientation of each of these grains is shown in Figure 1 to aid qualitative visualization of the crystal orientation of these grains. It can be seen that the orientation between the three selected grains are significantly different. Quantitative analysis on the EBSD data shows that the misorientation between any two of these three grains is more than about 35°. Typical nanoindentation curves obtained from each of the three grains that exhibit a significant pop-in are shown in Figure 3. It can be seen that the loading curves before the occurrence of a pop-in can be fitted with a Hertzian curve (using R~353 nm) and the indentation curve deviates from the

Hertzian fitted curve after the occurrence of a pop-in, suggesting that the observed pop-in indicates the onset of plastic deformation. There are at least 27 indentations from each grain that exhibit a pop-in having a significant displacement excursion. The rest of the indentation curves only demonstrated a change of slope in the loading part of the curve where it started to deviate from the Herzian behavior, indicating a transition from elastic to plastic deformation. The load at which a pop-in occurs and the associated displacement excursion observed from the nanoindentation curves obtained from each grain varies from indentation to indentation, demonstrating stochastic yielding behavior. Distributions of the observed pop-in load and displacement excursion at pop-in obtained from at least 27 indentations on each of the three grains are shown in Figure 4.

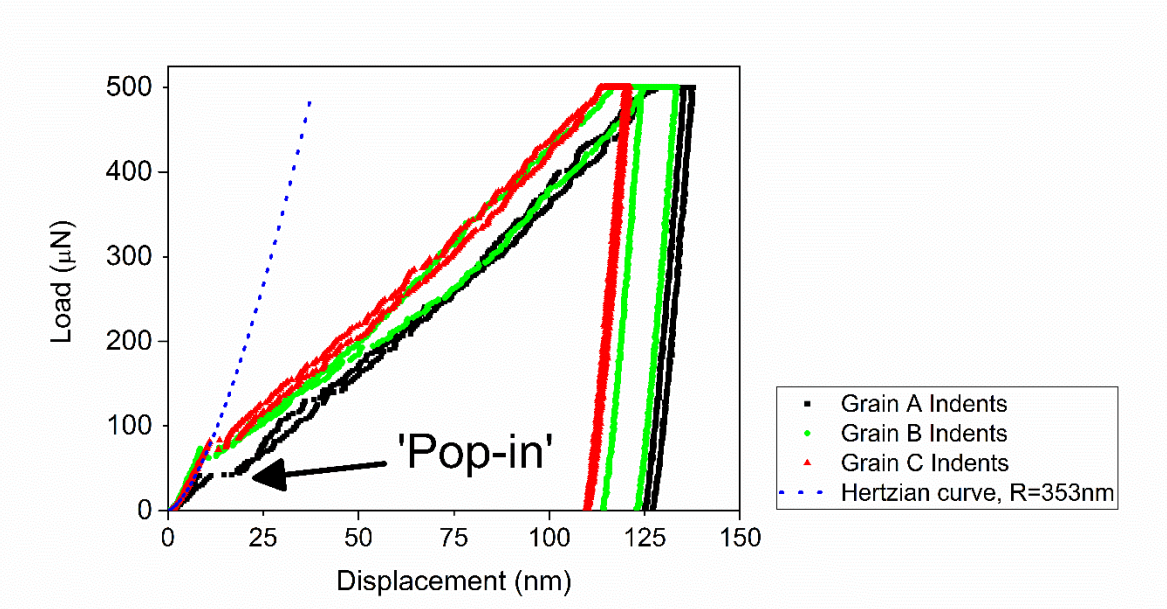

Figure 3. Typical indentation curves obtained from Grains A, B and C.

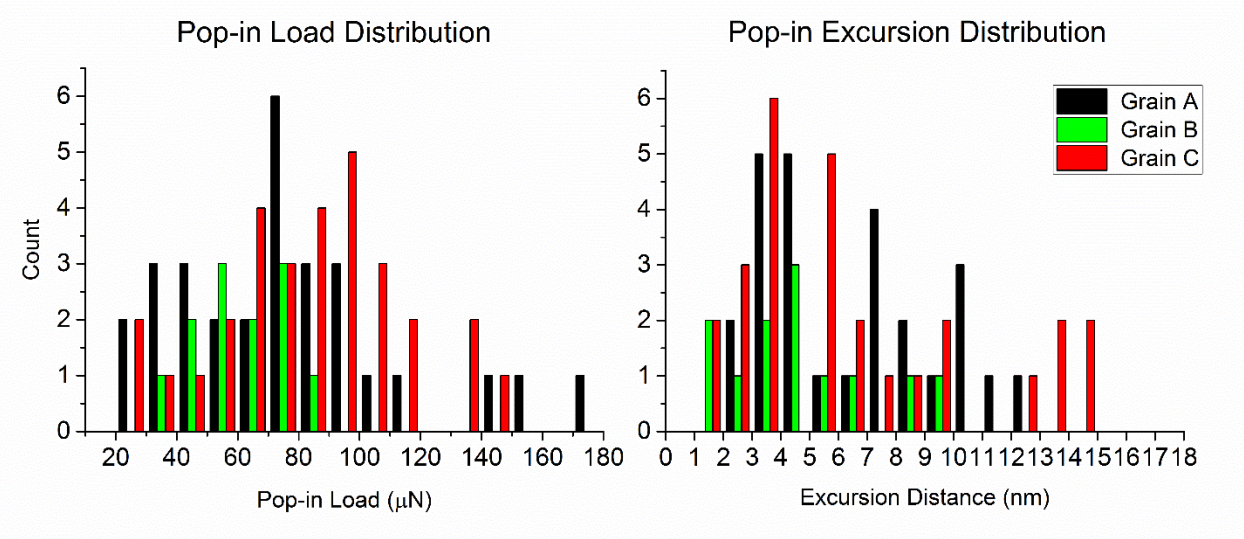

Figure 4: Pop-in load and excursion distributions of grains A-C.

Distributions of pop-in load and pop-in excursion for each grain can be qualitatively observed to be normal or skewed distributions. A skewed distribution has a mean value closer to zero and since a negative value is not possible for pop-in load or the associated displacement excursion these skewed distributions are treated as a normal distribution in the following analysis. It can be seen that the mean pop-in load for Grain B is apparently lower than that observed from Grains A and C. However, the mean displacement excursion at pop-in is about the same for all three grains. Table 1 shows the descriptive statistics including the mean and standard deviation regarding the distributions of the pop-in load and displacement excursions obtained from the respective grain tested.

Table 1: Mean values and standard deviations of the pop-in loads and displacement excursion at a pop-in obtained from Grains A, B and C.

	Pop-In Load (μN)	**Pop-in Excursion (nm)**
	Mean ±SD	Mean ±SD
Grain A	82.4 ±40.4 (n=52)	6.9 ±7.4 (n=52)
Grain B	59.3 ±25.6 (n=27)	4.9 ±2.8 (n=27)
Grain C	87.6 ±32.4 (n=44)	5.4 ±3.8 (n=44)

In order to quantitatively determine whether the mean of the pop-in load and the associated displacement excursion obtained from the three grains are significantly different or not, two-tailed t-tests were done between the three distributions obtained from Grain A, B and C. A t-test requires that the two data sets of interest involved each test are both normally distributed without significant outliers and for each set of data the minimum sample size, *n*, ranges between 25- 40 [17]. According to the results shown in Figure 4, t-test is an appropriate hypothesis testing method to be applied on the current sets of data. Assuming normality and equal variance conditions, the original null hypothesis states that the means of two sets of data being considered were equal and the alternative hypothesis states that the two means were not equal. The test statistic, t_0, can be calculated as [17]

$$t_0 = \frac{\bar{x}_1 - \bar{x}_2}{s_p\sqrt{\frac{1}{n_1}+\frac{1}{n_2}}} \quad (2)$$

where, $\bar{x}_1$ and $\bar{x}_2$ are the calculated averages of either pop-in load or displacement excursion of two compared grains, s_p is the pooled estimator, n_1 and n_2 are the sample sizes of the two grains being compared.

In order to determine the probability of the null hypothesis, the *p*-value of the test statistic will be compared to the significance level, $\alpha = 0.05$ (99.5% confidence level). When the null hypothesis is true, the *p*-value is the probability of obtaining a result at least as extreme as the one observed and so the criterion for rejection of the null hypothesis is $p < \alpha$. The *p*-values calculated from the value of t_0 for the pop-in load and displacement excursion distributions between the three grains are shown in Table 2. It can be seen that for $\alpha = 0.05$, i.e. 99.5% confidence level, the pop-in excursion observed in all three grains are not significantly different. In addition, the pop-in load are significantly different between Grains A and B and between Grains B and C. However, the pop-in load between Grains A and C are not significantly different.

Table 2: Result from two-tailed hypothesis testing between pairs of grains for significant level α = 0.05.

Pairs of grains in Comparison	Distributions being considered	
	Pop-in Load	**Pop-in Excursion**
Grain A - Grain B	p = 0.0084 Significantly different	p = 0.17 Not significantly different
Grain A - Grain C	p = 0.49 Not significantly different	p = 0.49 Not significantly different
Grain B - Grain C	p = 2.48E-4 Significantly different	p = 0.26 Not significantly different

Upon close inspections on the distributions of pop-in loads in Figure 4(a), the spread of the pop-in load distributions for the three tested grains appears slightly different, suggesting that the stochastic nature of onset of plasticity is affected by the grain orientations. The coefficient of variance (ratio of one standard deviation to the mean of a distribution) is the lowest for the distribution of pop-in events in Grain C amongst the three grains, suggesting that the spread of the pop-in load distribution is narrower in Grain C compared to Grain A and B. Similar observations of crystal orientation influence on the spread of pop-in event distributions has been reported in Ni and NiAl previously [13, 18]. The phenomenon was associated with the more pronounced influence of defects in certain orientations (for example (110) and (111) in Cu), in addition to the result of a tip with a larger radius creating a larger stress field that is more likely to include a larger number of bigger defects [13]. Further, the density of statistically stored dislocations and the presence of dislocation clusters in a grain may also be depending on crystal orientation as seen in TEM analysis on similar Cu samples in a prior work [19]. To get an insight of the dislocations distributions in Grain A, B and C, these three grains were isolated from the EBSD scans shown in Figure 1 and are configured to show the geometrically necessary dislocation (GND) density (Figure 5) within each of these grains. In order to do so, each point in the EBSD scan was compared to its first nearest neighboring points. The GND density was then calculated based on the lattice rotation. A tolerance of 5° was set for the presentation shown in Figure 5. It is worth to note that the EBSD scans were performed prior to the nanoindentation, so

Figure 5 represents the GND density of the as prepared sample. The mean GND densities for the three grains are very similar and are in the order of 10^{12} m^{-2}, which is an order of magnitude lower than the total dislocation density estimated from the TEM analysis. It is likely that the additional dislocation density comprised of statistically stored dislocations. The GND density near the grain boundaries is about 5 to 10 × 10^{12} m^{-2} higher than that measured within the interior of Grains A, B and C. Clusters of higher GND density can also be seen randomly distributed within the grains. Nanoindentation near or directly on these clusters may contribute to the stochasticity in the pop-in behavior. In addition, the small differences in the initial GND density in the three grains are unlikely to impose significant contribution toward the observed differences in the mean of pop-in load.

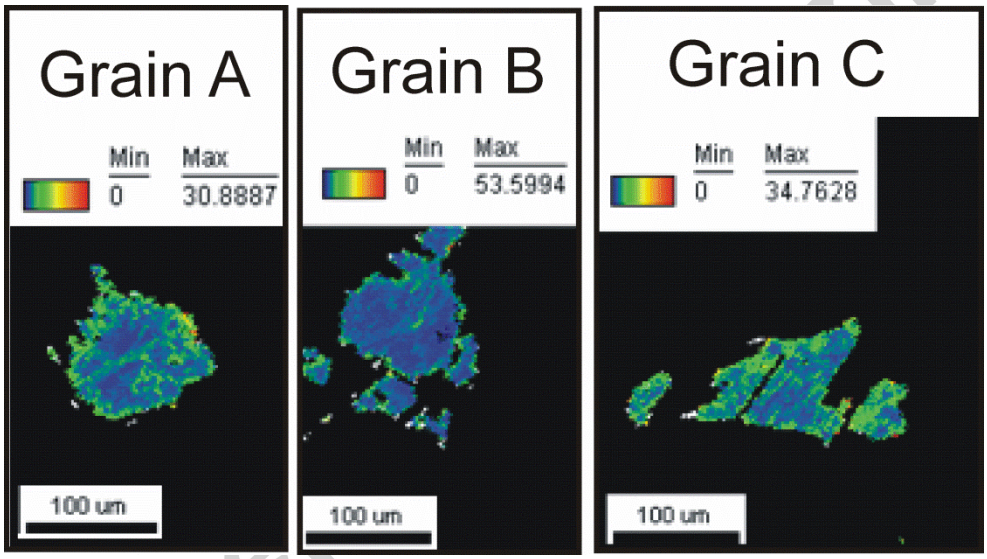

Figure 5. GND density presentation of Grains A, B and C extracted from the EBSD scan shown in Figure 1. Unit of the color scales in the above figures is 10^{12} m^{-2}.

In summary, the results of hypothesis testing above suggest that grain orientation affects the onset of plastic deformation during nanoindentation, in agreement with various reports from the literature, for example [13, 18]. In particular, Li *et al.* [18]} demonstrated the orientation dependency of pop-in load based on an indentation Schmid factor developed by these authors.

The pop-in load distributions shown in Figure 4(a) is plotted as a cumulative distribution of pop-in events against the maximum shear stress τ_{max} under the indenter at the pop-in load (Figure 6), which can be expressed as [15]:

$$\tau_{max} = 0.31 \cdot \left(\frac{6P_{pop-in}E^{*2}}{\pi^3 R^2}\right)^{\frac{1}{3}} \quad (3)$$

where P_{pop-in} is the pop − in load, R is the tip radius (353 nm) and E^* is the reduced modulus. The average value of E^* for Grain A, B and C are 90.9 ±6.5, 85.6 ±13.5 and 90.5 ±7.8 GPa, respectively. It can be seen that all three distributions obtained from the three grains exhibit a general 'S' shape, suggesting that there is a wide range of variations in the pop-in load. The similar shape of the distributions obtained from the three grains suggests that the occurrence of a pop-in is governed by the same mechanism. As discussed above, pop-in observed in a load-displacement curve obtained from nanoindentation on a relatively defect-free crystal is often associated with homogeneous dislocation nucleation underneath the indenter [6, 12, 20, 21] , which is a stress-assisted and thermally activated process. The rate of dislocation nucleation in a unit volume of material subjected to homogeneous shear stress τ can be written:

$$\dot{N} = N_0 \cdot exp\left(-\frac{\epsilon - \tau v^*}{\kappa T}\right) \quad (4)$$

where N_0 is the pre-exponential constant "attempt frequency", ϵ is the intrinsic nucleation energy barrier, $v^*$is the activation volume, κ is the Boltzmann constant and T is the absolute temperature. The shear stress τ in equation (4) can be taken as the maximum shear stress under the indenter at the pop-in and can be calculated using equation (3). Since only one initial yield event is possible for each indentation, the population of indentations available to yield is equal to 1-f [6]. A differential equation describing the population can be written:

$$\dot{f} = (1 - f)\dot{N} \quad (5)$$

The unknown parameters $v^*$and N_0 in equation (4) can be obtained by applying a linear least squares fitting of $\ln(\ln(1\text{-}f)^{-1})$ as a function of τ_{max} (Figure 7) [22]. Using a linear regression curve fitting, the two unknown parameters in equation (4) can be obtained from the slope, $\frac{v^*}{\kappa T}$ and the intercept $N_0 \cdot exp\left(-\frac{\epsilon}{\kappa T}\right)$, which is the rate of defect nucleation in a crystal due to thermal activation alone without stress application. The activation volumes v^* (in nm^3) normalized by the Burgers' vector (b_{Cu}=0.256 nm) obtained from the above analysis for the indentation pop-in events on Grains A, B and C are found to be 0.62b^3, 0.53b^3, and 0.72b^3, respectively. Using

similar analysis on the statistics of yield strengths in compressed micro-pillars and thin film under tension, Shao *et al.* [22] found that the activation volume for yielding linearly increases as the size of the micro-structure increases. The activation volume observed in the current experimental work is equivalent to that calculated for a micro-pillar having a small diameter (~ 100 nm) or a very thin film (~ 200 nm thick) when the deformation is likely dominated by the nucleation of new dislocations. The atomic level of the calculated activation volumes suggests that pop-in events are associated with the displacement of only one or two atoms, which cannot by itself explain the nanometer indentation displacements at the pop-in observed from the experiment. It is likely that pop-in events are associated with dislocation activities but have an atomic sized precursor. This was observed in MD simulation work by Ngan *et al.* [10, 11] on nanoindentation in Ni_3Al. It was observed that when the stress was about 90% of the critical value for pop-in, atomic clusters with relative displacements > 17% of lattice parameter started to form and resulted in a Shockley partial loop to emerge, which eventually forms a slip plane. The authors suggested that in reality the small Shockley partial loop may have evolved into other faults, which then cross-slip to form a Frank-Read source that lead to an observable displacement excursion. Other simulation work also show that dislocation can grow from atomic size volume where the crystal lattice buckled rather than from the nominal equilibrium size of a dislocation [21]. If the occurrence of a pop-in is related to dislocation generation that began from an atomic size volume, the stochasticity in pop-in load is then associated with the probability of atomic movements that lead to instability for dislocation formation. On the other hand, Lawrence *et al.* [8] also observed atomic size activation volume at pop-in from nanoindentation experiments on pure Ni using similar analysis. According to their observations, the authors suggested that pop-in may be associated with the propagation of dislocation instead of dislocation nucleation. As dislocations affected by the indentation stress field are likely not located symmetrically under the indenter tip, an activation event is required to assist the expansion of a dislocation loop once the stress on the entire loop is sufficient to move the dislocation. In this case, the stochasticity observed is related to the relative location of pre-existing dislocation under the indentation stress field. We believed that in reality there is a mixture of the above events that leads to a pop-in, depending on the distributions of faults and defects that pre-existing in the crystal. When there are no defects in the vicinity of the indentation, the atomic size precursor may be the mechanism

of pop-in, but when there are defects nearby, the activation of dislocation loop expansion is more likely to be the pop-in mechanism.

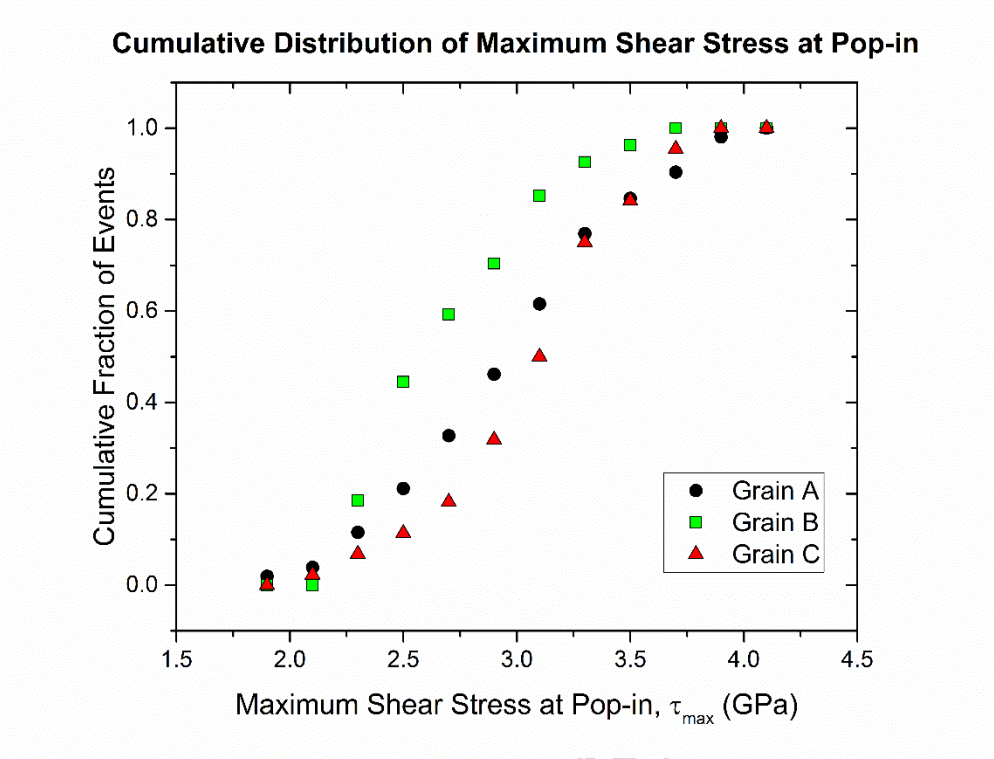

Figure 6. Cumulative frequency plot showing the probability of maximum shear stress at which the Pop-in occurs for each Grain A-C.

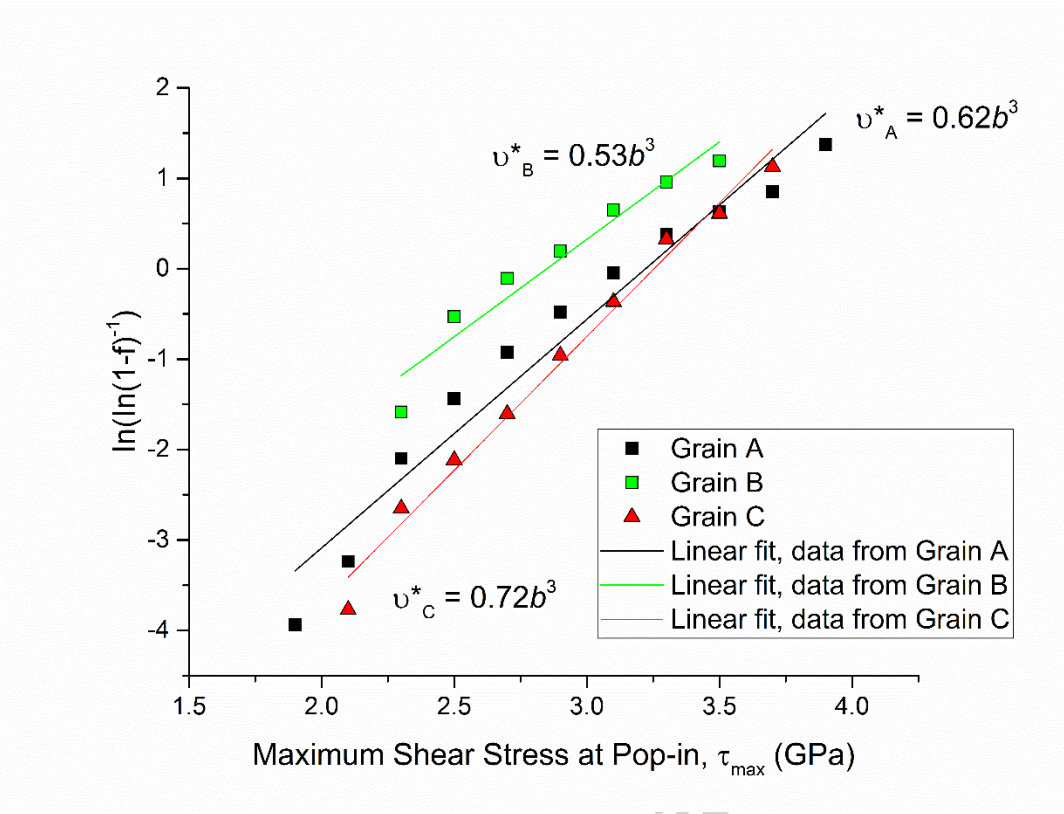

Figure 7. Data from Figure 6 replotted in a form that used for application of a linear least-squares fitting procedure to obtain the values of activation volume υ, value shown is normalized by the Burgers vector b.*

Effect of probe size on hardness

In order to study the influence of the size of the tip used during nanoindentation on the measured hardness, in addition to the *H* values that can be obtained from indentation using a probe having radius of ~ 353 nm shown in the previous sections, nanoindentation were also performed using a larger Berkovich tip. Using the curve fitting methods described above, the tip of the larger probe has a radius of ~ 2420 nm. The reason of performing this study is to examine how using different tips or the same tip with different degree of wear could affect the *H* measurements. At least 39 indents were made using each probe on each of the grains A, B and C. The hardness value measured from each indentation using the same probe on the same grain is found to be varying, reflecting the stochastic nature of nanoindentation hardness measurement. The distributions of hardness obtained from the three grains using the two probes are shown in Figure 8. It can be seen that when using the same probe on the same grain the *H* distribution is close to a normal distribution. The overall mean of *H* value for each grain appears lower when a

larger probe was used (see Table 3 and the dotted line across Figures 8 (a) and (b)) . Results of t-testing comparing *H* between the three grains using the two probes are shown in Table 4. It was found that the mean *H* of the three grains are not significantly different when a larger probe was used, but the mean *H* of the three grains are different when compared to the smaller probe, showing crystal orientation affects the *H* values when a smaller probe was used. However, *H* is not sensitive to crystal orientation when the larger probe was used. In addition, the coefficient of variance for the *H* distributions obtained using both probes are very similar, suggesting that *H* measurements using these two probes are subjected to similar stochasticity.

Table 3: Mean values and standard deviations of indentation hardness using the two Berkovich probes having different tip radii.

	Hardness (GPa)	
	Small Probe (R = 353 nm)	Large Probe (R = 2420 nm)
	Mean ±SD	Mean ±SD
Grain A	1.60 ±0.95 (n=41)	0.95 ±0.21 (n=63)
Grain B	1.48 ±0.34 (n=40)	0.80 ±0.27 (n=60)
Grain C	1.60 ±0.24 (n=41)	0.97 ±0.24 (n=64)

Table 4: Result from two-tailed hypothesis testing between H measurements obtained from pairs of grains and two different probes for significant level $\alpha = 0.05$.

Comparison pair		**Distributions being considered**	
		Small Probe (R = 353 nm)	**Large Probe (R = 2420 nm)**
Comparisons between grains using the same probe	**Grain A - Grain B**	p = 0.007 Significantly different	p = 0.213 Not significantly different
	Grain A - Grain C	p = 0.665 Not significantly different	p = 0.971 Not significantly different
	Grain B - Grain C	p = 0.001 Significantly different	p = 0.084 Not significantly different
Comparisons between probes on the same grain	**Grain A**	$p = 7.05 \times 10^{-13}$ Significantly different	
	Grain B	$p = 4.82 \times 10^{-16}$ Significantly different	
	Grain C	$p = 2.24 \times 10^{-24}$ Significantly different	

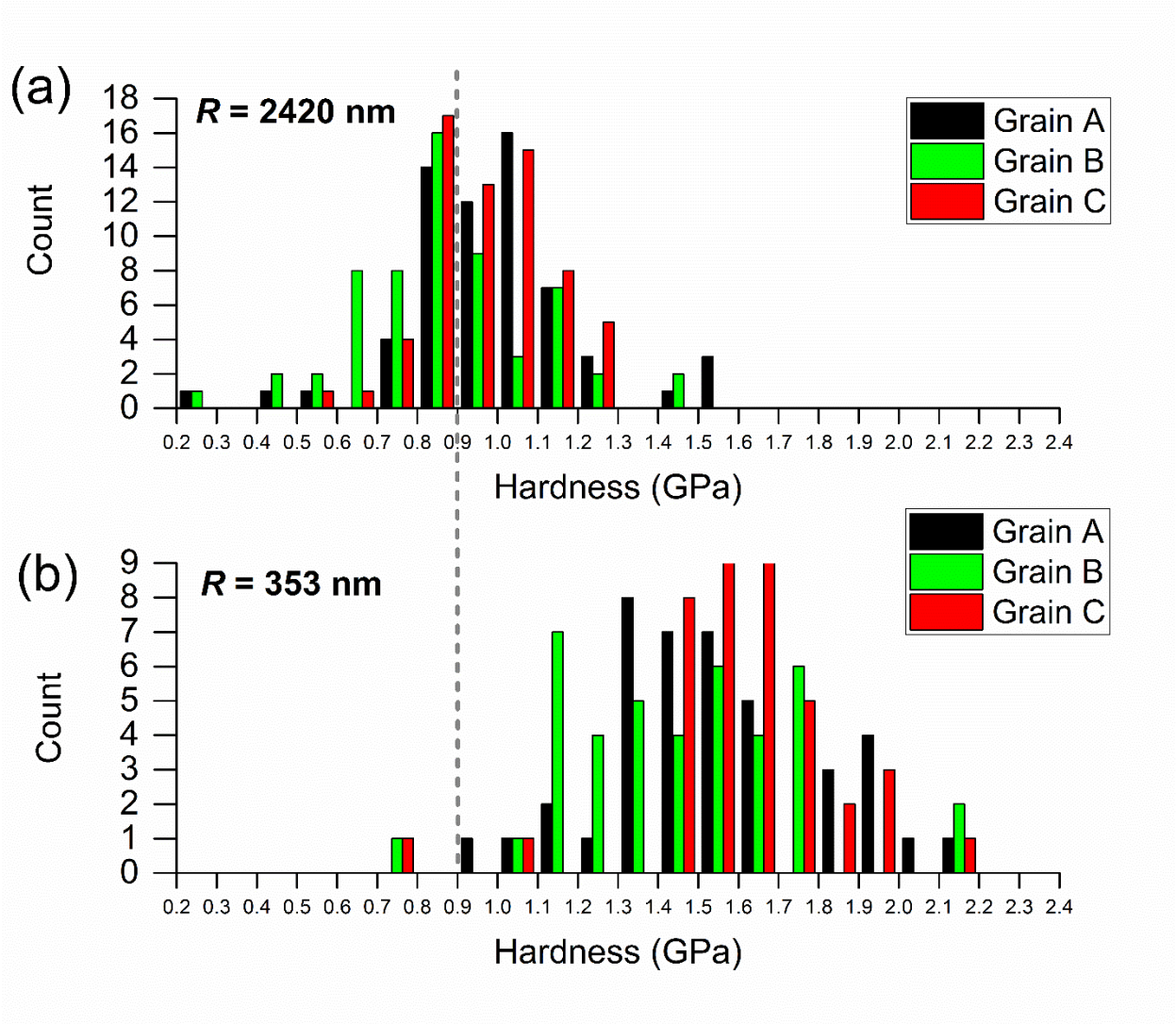

Figure 8: Frequency distributions of hardness values obtained from performing nanoindentation using two Berkovich probes having different radii (a) a large probe, R = 2420nm and (b) a smaller probe, R = 323nm.

Previous work by Lawrence *et al.* [8] and Salehinia *et al.* [13] has shown that indenter tip radius affects the onset of plasticity in such a way that there is less variations in the pop-in load when a smaller indenter was used and that when a larger indenter was used the pop-in load showed higher dependency on crystal orientations [13]. The indentation depth at pop-in is usually so shallow that only the round part of the indenter tip, regardless of the overall geometry, was in contact with the material. The *H* measurements, however, were obtained from the unloading nanoindentation data where in our case the indentation depth was beyond the part of the tip that could be approximated as spherical. Therefore, the observations from Figure 8 could be the results of indentation size effect (ISE), which is largely depending on the indentation

depth for a sharp indenter (typically higher *H* for shallower indents) and tip roundness for spherical tips (higher *H* for tip with smaller radius) [23-25]. In the current study, the two probes used have the same overall geometry (Berkovich tips) and the main difference is the tip roundness or sharpness of the tip. Under the same maximum applied load, it was observed that the sharper tip has a larger indentation depth of 125.5 ± 39.7 nm, whereas the indentation depth using a larger probe was 67.5 ± 13.2 nm, thus ISE may contribute to the higher *H* values obtained using the smaller probe. However, the measurements made with the larger tip may be subjected to more significant influence from the tip roundness as the indentation depth is very shallow. This may explain the current findings that a higher *H* results from a larger indentation depth, which is opposite to the typical ISE phenomena for a sharp indenter. In addition, when the deformation in the crystal is fully plastic, the effect of interactions between the indentation stressed volume and pre-existing internal defect structures manifests and results in the *H* having a stronger dependency on crystal orientation. As discussed earlier, TEM analysis on similar Cu sample suggested a dislocation density relatively high (in the order of 10^{13} m^{-2}) for a substantially annealed sample, a larger stressed volume that has higher density of geometrically necessary dislocations (GNDs) under the indenter created by the sharper indenter having deeper indentation depth is more likely to activate more dislocations in the crystals. It is possible that there were interactions between the indentation stressed volume and point defects such as vacancies, but the nanoindenter is likely not sensitive enough to show the influence from these interactions. The stochasticity on the nanoindentation *H* is therefore likely dominated by the activation of pre-existing dislocations after the crystal was plastically deformed.

Effect of Grain Boundary on Hardness

The above statistical analysis on the pop-in events and hardness observed in relatively defect-free crystals agrees with various reports from the literature that intrinsic properties of a crystalline material, including orientations and the presence of internal structural defects in a crystal affect the stochastic behavior of plastic deformation. In this section, the influence of grain boundaries as a specific type of crystal defect on the plastic deformation stochasticity is explored. It is known that grain boundaries can affect dislocation movement across them [26-28] but the extent at which the grain boundary directly affects mechanical properties in the sub-

micron scale is largely unclear. In order to study how grain boundaries contribute to the stochastic nature of plasticity in a polycrystalline Cu crystal in the sub-micron scale, nanoindentation hardness were measured near (< 2.5 μm from) a grain boundary as well as at various further distances measured perpendicular to this boundary. A SEM micrograph showing the grain boundary and most of the indents made on the two adjacent grains tested are exhibited in Figure 9(a). The two grains associated with this selected grain boundary are labeled X and Y. These two grains are indicated in the IPF presentation of an EBSD scan of the sample in Figure 9 (b), which also includes grains in the surrounding area. Grains X and Y were chosen without a specific favoring of crystal orientation or misorientation between them. According to the EBSD results, the normal of the grains X and Y are [-6 -1 28] and [-24 1 -28], respectively and the misorientation between these two grains is found to be ~ 58°. A total of 28 indentations were made on Grain X and Y. The hardness of indentations were calculated from the unloading segment of the nanoindentation curve using the Oliver-Pharr method [29]. The distance of an indent from the grain boundary is the length measured from the SEM image and is defined as a perpendicular distance from the boundary to the center of the residual imprint of an indentation. Figure 10 shows a plot of hardness of indentations and their corresponding distance from the grain boundary that locates between grains X and Y. The *H* value obtained > 5 μm from the grain boundary on both Grains X and Y scattered about the same average value of ~ 1.5 GPa. It can be seen in the SEM image (Figure 9(a)) that one of the indent was made on the grain boundary. Hardness value was not able to be measured from this data point, likely due to the uneven surface at the slightly etched grain boundary.

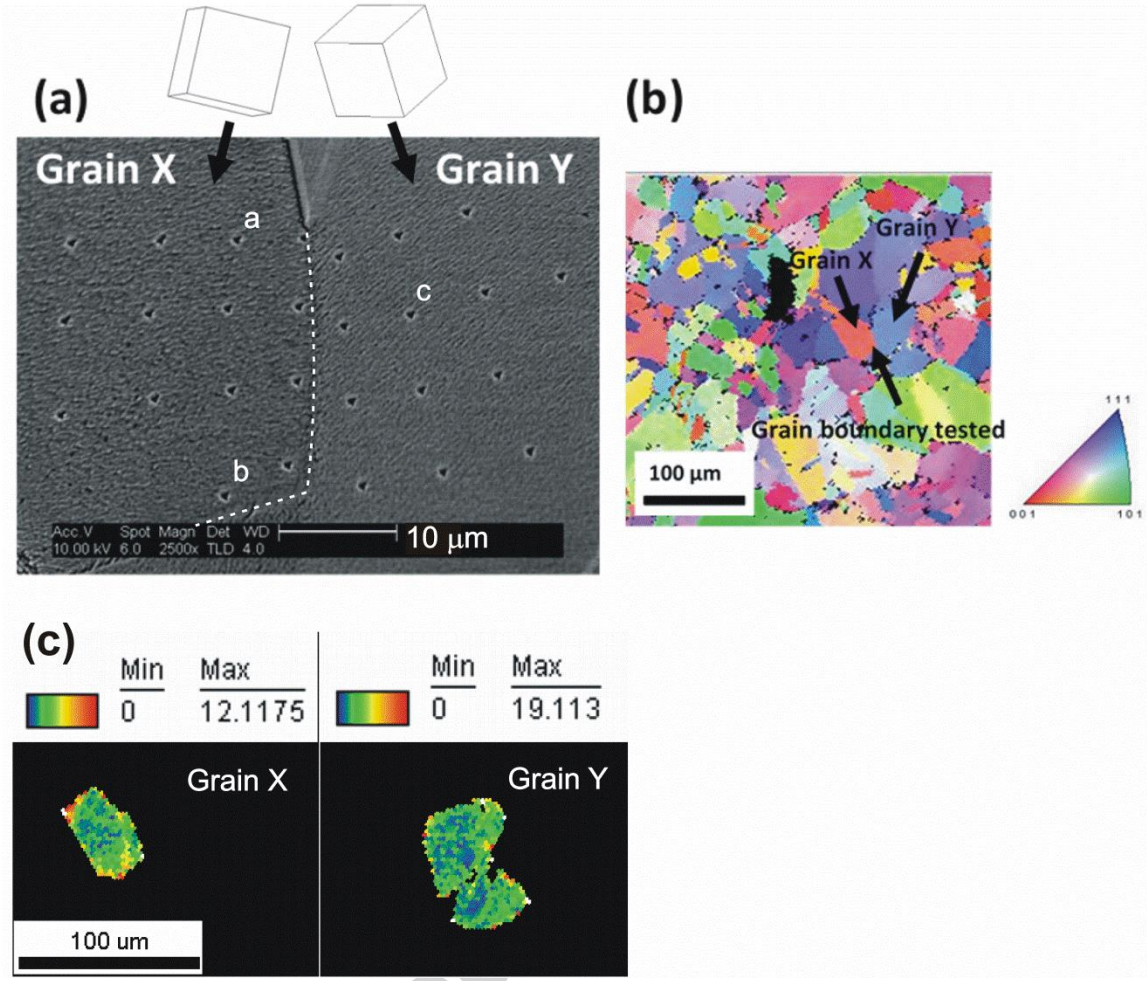

Figure 9(a) SEM micrograph showing the grain boundary of interest and the imprint of nanoindentations made around this grain boundary. The dotted line illustrates a continuous grain boundary between the two grains. (b) IPF representation of an EBSD scan of an area including the location of this tested grain boundary.(c) GND density presentations of Grain X and Y extracted from the EBSD scan shown in (b). Unit of the color scales in figure (c) is 10^{12} m^{-2}.

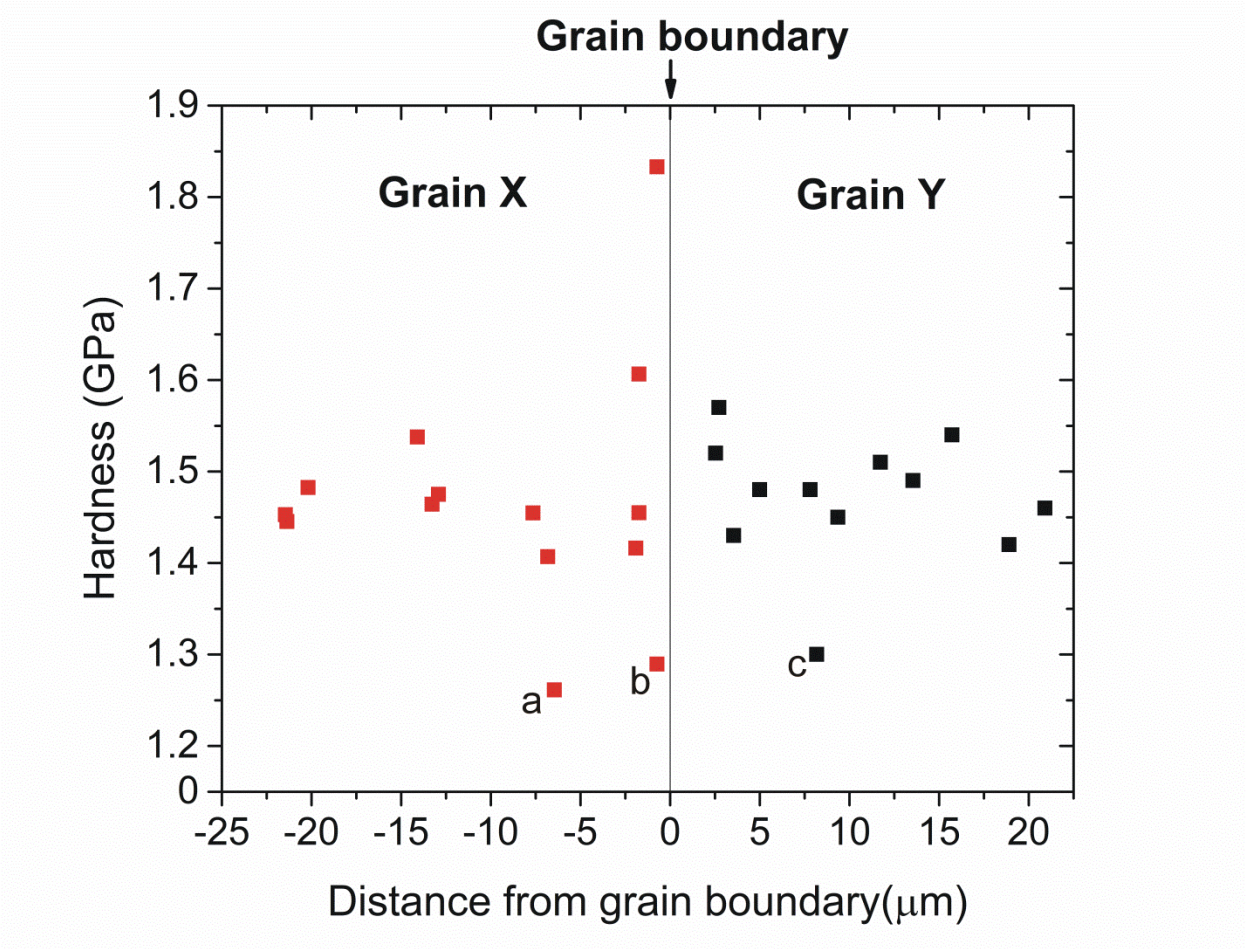

Figure 10: Hardness versus distance from the Grain X-Grain Y boundary. The vertical axis at x=0 represents the grain boundary. Each point corresponds to the hardness value from a single indent.

As approaching the grain boundary on Grain X and at distances less than ~ 2 μm away, the hardness values appears to rapidly reach a peak value of ~ 1.83 GPa at about 1 μm from the grain boundary. This value is ~ 0.4 GPa (~ 27%) higher than the average value measured from nine data points > 5 μm from the grain boundary (1.44 GPa), showing an apparent grain boundary hardening effect. Within Grain Y, however, the closest indentation to the grain boundary was made at 2.54 μm, so if there is a grain boundary effect similar to that observed in Grain X, such grain boundary hardening effect is not observable in Grain Y. Similar grain boundary hardening effects has been observed in other bicrystals or polycrystals, for example [27, 28] most of these studies attribute this grain boundary hardening effect to dislocation pile up at the grain boundary that triggers the nucleation of sources in the adjacent grain as those

experimental results could be described by the Hall-Petch relationship. It is worth to note that three data points in Figure 10 show significantly lower *H* values from the mean at ~ 1.3 GPa. These data points are indicated as 'a', 'b' and 'c' in Figure 10 and the corresponding indents are also labeled in the SEM image shown in Figure 9(a). The data point 'b' that associated with a *H* value of 1.28GPa should be discarded as according to the SEM image the relative orientations between the probe and the grain boundary is different from all the other indents. The other two isolated lower *H* measurements 'a' and 'c' do not appear to be related to observable structural features or defects in the SEM image. In order to explain the higher hardness values obtained near the grain boundary (< 2.5 μm) and the lower *H* measurements further away from the grain boundary shown in Figure 10, grain boundaries of polycrystalline Cu samples prepared using a similar method as those used for indentations were studied in the TEM. It can be seen in Figure 2(b) that there are networks of dislocations neatly arranged forming a rather straight band that has a finite width of ~ 125 nm across the top and bottom within the field of view. As discussed above, diffraction analysis in this area confirmed that orientation of the grains on the two sides of this band of dislocations is different, meaning that the grain boundary lies within this band of dislocations. A few individual dislocations can also be identified outside the band of dense dislocations. These dislocations around the grain boundary will lead to a higher dislocation density in the proximity of the grain boundary compared to the dislocation density estimated within the grain at ~ 2×10^{13} m^{-2}. Similar treatment on the EBSD scan to shown GND density as discussed above was done for the EBSD scan that includes Grain X and Y (Figure 9(c)). It can be seen that the GND density is higher near the grain boundaries of Grain X and Y. This observation also agrees with the TEM observations that dislocation density is higher along a grain boundary. Note that the step size of the EBSD scan was 2.25 μm, so the fine differences in GND density near the grain boundary that may lead to the apparent grain boundary hardening observed in Grain X may not be resolved. The higher dislocation density at and near the grain boundary likely lead to a higher nanoindentation hardness value due to strain hardening effect as a result of dislocation interactions between the GND within the indentation plastic zone and those pre-existing in the crystal near and at the grain boundary. On the other hand, the randomness of isolated and localized dislocations or their clusters existing around the grain boundary could lead to a degree of stochasticity in *H* measurement and hence the lower *H* values measured at locations 'a' and 'c' as seen in Figures 9 (a) and Figure 10. Hardness is defined as

the resistance of a material to plastic deformation, thus any microstructural feature that can hinder or assist the mobility of dislocations can raise or lower the hardness of the material. Although the exact radius of plastic deformation zone created by an nanoindentation is not known in this sample, it can be estimated to be approximately three times the radius of the indentation according to a prior direct observation of the plastic deformation zone around nanoindents made in a Ni_3Al crystal [30]. The radius of the indentation made at P_{max} = 500 μN in this study is ~ 0.5 μm (Figure 9(a)), thus the indents which are < 1 μm away from the grain boundary are likely to have dislocations from their plastic deformation zone in interaction with certain dislocation clusters near the grain boundary, leading to a higher hardness values as the indentation is closer to the grain boundary from Grain X approaching to the grain boundary. However, as seen in Figure 2(b), the concentration of dislocation does not reduce in a graduate manner away from a grain boundary. The hardening effect would be manifested if the dislocation pile-up running into a significant cluster of pre-existing dislocations. On the other hand, grain boundary hardening effect may not be observable if the dislocation pile-up induced by a nanoindentation does not encounter additional dislocations around the grain boundary. In other words, the pre-existing dislocation clusters that appear to be highly concentrating near grain boundaries may lead to stochasticity in hardness measurement and provide a plausible explanation to the contradicting observations from the other side of the grain boundary, i.e. from Grain Y approaching to the grain boundary (Figure 10). In addition, similar nanoindentation experiments in the literature usually include limited indentation near a small number of grain boundaries, the small sampling size in each study and the stochastic nature of grain boundary hardening effect as described above may then lead to different conclusions such that grain boundary hardening effect was significant in some studies [27, 28] whereas it is not observable in others for example [26]. In a recent work by the current authors [19], nanoindentation experiments on Cu showed that a lower *H* was observed when slip transferred across a grain boundary while a higher *H* was observed when a higher concentration of GND was observed between an indent and a grain boundary, suggesting that slip blockage lead to a higher *H* value. A dislocation density based model developed that predicts slip transmission at a grain boundary also suggested that the dislocation flux, i.e. the differences in initial dislocation densities between the neighboring grains is an important factor for intergranular slip transmission, which affects the grain boundary hardening effect.

Conclusions and summary

Nanoindentation was carried out on an annealed, electropolished high purity polycrystalline Cu to study the influence of microstructures on the stochastic mechanical responses in the material during nanoindentation. It was found that:

1. Hypothesis testing on the statistics of pop-in load showed that spreads and variations of data were different for nanoindentation made on different grains of arbitrary orientations, suggesting that crystal orientation contributes to stochasticity in the onset of plasticity.
2. Activation volume analysis applied to the pop-in load statistics was found to be of atomic size. The atomic size activation volume could be a precursor for dislocation nucleation in a dislocation depleted stressed volume of the indent or dislocation propagation in the present of dislocations within or near the indentation stressed volume.
3. It was found from the nanoindentation tests carried out on the same grain using two Berkovich probes having about one order of magnitude difference in tip radius that the hardness obtained by both tips demonstrated stochasticity, but the *H* obtained using a smaller tip is significantly higher than that measured from the larger tip. This may be due to a combined effect of indentation size effect and the likelihood that more defects were sampled in a highly stressed and larger stressed volume associated with indents made with the smaller probe. In addition, the hardness measured using the larger tip was not sensitive to crystal orientation, but using the smaller tip showed sensitivity to crystal orientation.
4. Hardness measured from either side of an arbitrary chosen grain boundary showed significant stochasticity. An apparent grain boundary hardening effect was observed only on one side of the grain boundary. The hardening effect may be explained by the interaction between the geometrically necessary dislocations from the indent made close to the grain boundary and the dislocations that decorate along the grain boundary as observed from transmission electron microscopy and GND density analysis from the EBSD data. Significantly lower *H* values were also measured at isolated locations slightly further away the grain boundary which may be the result of different defect distributions in those localized areas, these data points clearly demonstrate the stochastic

nature of *H* measurements near a grain boundary that may be originated from the presence of higher density of randomly distributed defects in these area.

Acknowledgement

Funding: This work was supported by the National Science Foundation [grant numbers CMMI 1434879]. BJS would like to thank NSF/CMMI for the REU supplement support. TEM images were obtained from the Franceschi Microscopy and Imaging Center at Washington State University.

References

[1] P. Sudharshan Phani, K.E. Johanns, E.P. George, G.M. Pharr, A stochastic model for the size dependence of spherical indentation pop-in, J. Mater. Res., 28 (2013) 2728-2739

[2] P. Pedro, R. Antonio, L. Silvia, T. Enrico, S. Karl, Role of Dislocation Density on the Sample-Size Effect in Nanoscale Plastic Yielding, J. of Nanomechanics and Micromechanics, 2 (2012) S1-S6

[3] J.R. Morris, H. Bei, G.M. Pharr, E.P. George, Size Effects and Stochastic Behavior of Nanoindentation Pop In, Physical Review Letters, 106 (2011) 165502

[4] M.R. Maughan, H.M. Zbib, D.F. Bahr, Variaion in the nanoindenation hardness of platinum, J. Mater. Res., 28 (2013) 2819-2828

[5] Y.L. Chiu, A.H.W. Ngan, Time-dependent characteristics of incipient plasticity in nanoindentation of a Ni3Al single crystal, Acta Materialia, 50 (2002) 1599-1611

[6] A. Schuh, A.C. Lund, Application of nucleation theory to the rate dependence of incipient plasticity during nanoindentation, J. Mater. Res., 19 (2004) 2152-2158

[7] A.M. Minor, S.A.S. Asif, Z. Shan, E.A. Stach, E. Cyrankowski, T.J. Wyrobek, O.L. Warren, A new view of the onset of plasticity during the nanoindentation of aluminium, Nature Materials, 5 (2006) 697-702

[8] S.K. Lawrence, D.F. Bahr, H.M. Zbib, Crystallographic orientation and indenter radius effects on the onset of plasticity during nanoindentation, Journal of Materials Research, 27 (2012) 3058-3065

[9] A.H.W. Ngan, L. Zuo, P.C. Wo, Probabilistic nature of the nucleation of dislocations in an applied stress field, Scripta Materialia, 54 (2006) 589-593

[10] P.C. Wo, L. Zuo, A.H.W. Ngan, Time-dependent incipient plasticity in Ni3Al as observed in nanoindentation, J. Mater. Res., 20 (2005) 489-495

[11] A.H.W. Ngan, L. Zuo, P.C. Wo, Size dependence and stochastic nature of yield strength of micron-sized crystals: a case study on Ni3Al, Proceedings of the Royal Society A - Mathematical Physical and Engineering Sciences, 462 (2006) 1661-1681

[12] Y.L. Chiu, A.H.W. Ngan, Time-dependent characteristics of incipient plasticity in nanoindentation of a Ni3Al single crystal, Acta Materialia, 50 (2002) 1599-1611

[13] I. Salehinia, S.K. Lawrence, D.F. Bahr, The effect of crystal orientation on the stochastic behavior of dislocation nucleation and multiplication during nanoindentation, Acta Materialia, 61 (2013) 1421-1431

[14] A. Akarapu, H.M. Zbib, D.F. Bahr, Analysis of heterogeneous deformation and dislocation dynamics in single crystal micropillars under compression, Int. J. Plasticity, 26 (2010) 239-257

[15] K.L. Johnson, Contact Mechanics, Cambridge University Press, Cambridge, UK, 1987.

[16] P. Schall, M. Feuerbacher, M. Bartsch, U. Messerschmidt, K. Urban, Dislocation density evolution upon plastic deformation of Al-Pd-Mn single quasicrystals, Philosophical Magazine Letters, 79 (1999) 785-796

[17] D.C. Montgomery, Engineering statistics, 4th ed. ed., Hoboken, NJ : John Wiley, Hoboken, NJ, 2007.

[18] T.L. Li, Y.F. Gao, H. Bei, E.P. George, Indentation Schmid factor and orientation dependence of nanoindentation pop-in behavior of NiAl single crystals, Journal of the Mechanics and Physics of Solids, 59 (2011) 1147-1162

[19] M. Hamid, H. Lyu, B.J. Schuessler, P.C. Wo, H.M. Zbib, Modeling and characterization of grain boundaries and slip transmission in dislocation density based crystal plasticity, Crystals, 7 (2017) 152-172

[20] C.L. Kelchner, S.J. Plimpton, J.C. Hamilton, Dislocation nucleation and defect structure during surface indentation Phys. Rev. B., 58 (1998) 11085-11088

[21] J. Li, K.J. Van Vliet, T. Zhu, S. Yip, S. Suresh, Atomistic mechanisms governing elastic limit and incipient plasticity in crystals, Nature, 418 (2002) 307-310

[22]S. Shao, N. Abdolrahim, D.F. Bahr, G. Lin, H.M. Zbib, Stochastic effects in plasticity in small volumes, International Journal of Plasticity, 52 (2014) 117-132

[23]J.G. Swadener, E.P. George, G.M. Pharr, The correlation of the indentation size effect measured with indenters of various shapes, J. Mechanics and Phys. of Solids, 50 (2002) 681-694

[24]G. Feng, W.D. Nix, Indentation size effect in MgO, Scripta Materialia, 51 (2004) 599-603

[25]W. Chen, M. Li, T. Zhang, Y.-T. Cheng, C.-M. Cheng, Influence of indenter tip roundness on hardness behavior in nanoindentation, Mater. Sci. and Eng. A, 445-446 (2007) 323-327

[26]P.C. Wo, A.H.W. Ngan, Investigation of slip transmission behavior across grain boundaries in polycrystalline Ni3Al using nanoindentation, J. Mater. Res., 19 (2004) 189-201

[27]W.A. Soer, J.T.M. De Hosson, Detection of grain-boundary resistance to slip transfer using nanoindentation, Materials Letters, 59 (2005) 3192-3195

[28]Y.M. Soifer, A. Verdyan, M. Kazakevich, E. Rabkin, Nanohardness of copper in the vicinity of grain boundaries, Scripta Materialia, 47 (2002) 799-804

[29]W.C. Oliver, G.M. Pharr, An improved technique for determining hardness and elastic modulus using load and displacement sensing indentation experiments, Journal of Materials Research, 7 (1992) 1564-1582

[30]P.C. Wo, A.H.W. Ngan, Y.L. Chiu, TEM measurement of nanoindentation plastic zones in Ni3Al, Scripta Materialia, 55 (2006) 557-560